

Silicon Planar Technology for Single-Photon Optical Detectors

E. Sciacca^a, A. C. Giudice^b, D. Sanfilippo^c, S. Lombardo^a, F. Zappa^b, R. Cosentino^d, M. Mazzillo^c,
M. Ghioni^b, G. Fallica^c, M. Belluso^d, G. Bonanno^d, S. Cova^b, E. Rimini^a.

^a CNR-IMM, Catania, Italy

^b Dipartimento di Elettronica e Informazione, Politecnico di Milano, Milan, Italy

^c R&D DSG STMicroelectronics Stradale Primosole 50 Catania, Italy

^d Osservatorio di Astrofisica, Catania, Italy

ABSTRACT

In this paper we report the results relative to the design and fabrication of Single Photon Avalanche Detectors (SPAD) operating at low voltage in planar technology. These silicon sensors consist of pn junctions that are able to remain quiescent above the breakdown voltage until a photon is absorbed in the depletion volume. This event is detected through an avalanche current pulse.

Device design and critical issues in the technology are discussed.

Experimental test procedures are then described for dark-counting rate, afterpulsing probability, photon timing resolution, quantum detection efficiency. Through these experimental setups we have measured the electrical and optical performances of different SPAD technology generations. The results from these measurements indicate that in order to obtain low-noise detectors it is necessary to introduce a local gettering process and to realize the diode cathode through in situ doped polysilicon deposition. With such technology low noise detectors with dark counting rates at room temperature down to 10c/s for devices with 10 μ m diameter, down to 1kc/s for 50 μ m diameter have been obtained.

Noticeable results have been obtained also as far as time jitter and quantum detection efficiency are concerned.

This technology is suitable for monolithic integration of SPAD detectors and associated circuits. Small arrays have already been designed and fabricated. Preliminary results indicate that good dark count rate uniformity over the different array pixels has already been obtained.

Keywords: planar technology, single photon detectors, photon counting, quantum efficiency.

1. INTRODUCTION

Photon counting and photon-timing are widely used measurement techniques, employed for weak and/or fast optical signals, luminescent [1] or fluorescent decays [2], optical fiber characterization [3], non-invasive testing of VLSI circuits [4] and laser ranging [5], photon correlation spectroscopy [6] and high energy physics experiments [7]. The suitable detectors must provide, in response to single photons, output signals that are sufficiently high to be individually processed by electronic circuits. Therefore, only detectors with an internal mechanism that provides a high multiplication of charge carriers are suitable, namely vacuum tube photomultipliers (PMTs) and solid-state avalanche photodiodes (APDs).

In PMTs, the available photocathodes for the visible spectral range provide fairly good quantum detection efficiency and low noise, that is, low dark-counting rate, whereas cathodes for the red and near-infrared range have lower quantum efficiency and must be cooled for reducing the dark-counting rate. The intrinsic time resolution obtained in photon timing with PMTs ranges from 1ns in ordinary PMTs to less than 30ps in ultrafast micro-channel plate multipliers (MCPs) [8]. PMTs are bulky, fragile, sensitive to electromagnetic disturbances and mechanical vibrations, require high supply voltages (2-3 kV) and are costly devices, particularly the high-performance models. Semiconductor APDs have the typical advantages of solid state devices (small size, low bias voltage, low power consumption, ruggedness and reliability, suitability to build integrated systems, etc.). Their quantum detection efficiency is inherently higher, particularly in the red and near infrared range. In APDs operating in linear mode the internal gain is not sufficient or barely sufficient to detect single photons. However, single photons can be efficiently detected by avalanche diodes operating in Geiger-mode, known as Single-Photon Avalanche Detector, SPAD.

2. DEVICE WORKING PRINCIPLE AND MAIN ISSUES

SPADs are p-n junctions operating biased at a voltage V_A above the breakdown voltage V_B . At this bias, the electric field is so high that a single charge carrier injected in the depletion layer can trigger a self-sustaining avalanche. The current swiftly rises with nanosecond or subnanosecond risetime to a macroscopic steady level in the milliamperere range, which can be easily discriminated. If the primary carrier is photogenerated, the leading edge of the avalanche pulse marks the arrival time of the detected photon. After the avalanche is triggered, the current keeps flowing until the avalanche is quenched by lowering the bias voltage down to V_B or below. The bias voltage is then restored in order to detect another photon. This operation requires a suitable circuit that is usually referred to as a quenching circuit [10].

As it happens in PMT's, thermal generation effects produce current pulses even in the absence of illumination, and the Poissonian fluctuation of these dark counts represents the internal noise source of the detector. The dark-count rate includes primary and secondary pulses [10]. Primary dark pulses are due to carriers thermally generated in the SPAD junction, so that the count rate increases with the temperature as does the dark current in ordinary photodiodes. The rate also increases with the overvoltage, $V_{over} = (V_A - V_B)$, because of two effects: i) field-assisted enhancement of the emission rate from generation centers [11] and, ii) increase of the avalanche triggering probability [12].

Secondary dark pulses are due to afterpulsing effects that may strongly enhance the total dark count rate. During the avalanche some carriers are captured by deep levels in the junction depletion layer and subsequently released with a statistically fluctuating delay, whose mean value depends on the deep levels actually involved [13]. Released carriers can retrigger the avalanche, generating afterpulses correlated with a previous avalanche pulse. The number of carriers captured during an avalanche pulse increases with the total number of carriers crossing the junction, that is, with the total charge of the avalanche pulse. Therefore afterpulsing increases with the delay of avalanche quenching and with the current intensity, which is proportional to the overvoltage. The value of V_E is usually dictated by photon detection efficiency or time resolution requirements, or both [10], so that the trapped charge per pulse first has to be minimized by minimizing the quenching delay.

If the trapped charge cannot be reduced to a sufficiently low level, a feature of the AQC can be exploited for reduction of the afterpulsing rate to a negligible or at least an acceptable level. By deliberately maintaining the voltage at the quenching level for a well defined hold-off time after quenching, the carriers released are prevented from retriggering the avalanche. However this strategy increases the detector dead-time, thus degrading the performance at high counting rate. The situation is even more disadvantageous when the detector is cooled to reduce the dark-counting rate, since the release from trapping states becomes slower.

In conclusion, a really suitable technology for producing SPADs must not only reduce the G-R centers to very low concentration level, but also eliminate trapping level or at least minimize their concentration. The technological challenge is to design a process with such characteristics and still compatible with standard microelectronic industry processes for IC production.

3. FABRICATION AND STRUCTURAL CHARACTERIZATION

Fig. 1 shows the cross-section of the SPAD structure. The n+p junction has a n+ shallow diffusion and a controlled Boron enrichment diffusion in the central zone of it. With respect to the outer abrupt n+p junction, the higher p+ doping concentration reduces the breakdown voltage in the central zone, which is the active area [14]. In order to obtain devices with low noise and wide active area, that is, with diameter of 50 μm or more, the original process flow [14] was redesigned.

The process starts with a Si <100> n- substrate on which we grow a boron doped epitaxial layer with a p+ buried layer and with a p- doped layer. The reason to form a buried p-n junction is twofold. First, the detector time-response (see Sec. 6) is improved because the effect of photogenerated carriers diffusing in the undepleted region is reduced [15]. Second, isolation with the substrate is introduced and makes possible the monolithic integration of various SPADs and other devices and circuits. The p+ buried layer is necessary to reduce the series resistance of the device.

The p- layer must be thin enough to limit the photocarrier diffusion effect above mentioned. A good trade-off has to be found for this thickness, because if it is made too thin the edge breakdown occurs at a voltage not much higher than the

breakdown voltage of the active area. The p++ sinkers are then created with a high-dose boron implantation step, in order to reduce the contact resistance of the anode and provide a low resistance path to the avalanche current.

The next step, a local gettering process, is a key step in the process and was introduced in the last recipe. At this point of the process a heavy POCl₃ diffusion through an oxide mask is made on the topside of the wafer close to the device active area. Heavy phosphorus diffusions are well known to be responsible for transition metal gettering [16]. Unfortunately the well known phosphorous predeposition on the backside of the wafer is not able to getter the distant active area of the device because metal diffusers (Pt, Aus, Ti) diffuse too slowly during the final anneal (700° C for 8 hours). For this reason, if the gettering sites are created suitably close to the active region, a major improvement is observed.

The next step is the p+ enrichment diffusion obtained with a low energy boron implantation, producing a peak concentration of $5 \times 10^{16} \text{ cm}^{-3}$, followed by a high temperature anneal and drive in [14].

The first generation of devices was fabricated with a deposited polysilicon cathode doped by Arsenic implantation and diffusion. The As+ ion implantation energy was carefully calculated in order to damage as little as possible the active area of the device; nevertheless, devices with very high dark-counting rate resulted. A remarkable improvement was obtained in the second generation by doping “in situ” the polysilicon. Further improvement was achieved in the third generation by accurately designing a Rapid Thermal Anneal to create a precisely controlled shallow Arsenic diffusion below the polysilicon in the p- epilayer. The final net doping profile has been measured by spreading profiling and it is shown in Fig. 2.

An important issue for the SPAD quality is the uniformity of the electric field over the active area. If the electric field is not uniform, the quantum detection efficiency (QE) of the device becomes dependent on the absorption position over the active area. The lower the electric field the lower the QE, the worst case being when the electric field is lower than the breakdown value. In order to check the quality of the fabricated photodetectors we used Emission Microscopy measurement. Typically this kind of measurement is performed at constant current, but because we want to check the situation well above the breakdown, the SPADs under test were observed in operation at 5V above breakdown, with an active quenching circuit. In Fig. 3 the three generations (recipes) of SPADs are compared. It is evident that for the last generation this figure of merit is very good. There are no hot spots indicating clusters of defects as in the first generation, and we observe very good uniformity in the breakdown voltage.

4. DETECTOR INTERNAL NOISE: DARK-COUNTING RATE

The basic goal of the SPAD fabrication technology is to keep low the primary dark-counting rate C_{th} due to the thermal generation of carriers; in fact, its statistical fluctuations are the basic internal noise source in a SPAD. In operating conditions, however, the effect of trapping and delayed release of avalanche carriers (see Sec.5) enhances the total dark-counting rate $C_{m,dark}$ to a level significantly higher than the primary rate C_{th} [10][13]. Carriers, trapped during an avalanche pulse and released with delay greater than the detector dead-time, re-trigger the avalanche and generate correlated after-pulses. A specific procedure was adopted for measuring the primary dark-counting rate, net from afterpulsing effects. The bias voltage given to the SPAD was a DC level plus a square wave, such that the bias was below BV in a half-period and well above BV in the other one. The two half-periods had equal long values, ranging from one to a few hundred milliseconds. A digital oscilloscope (Fig. 4) connected to a PC for data processing, measured the time from start of the high-level to onset of an avalanche current pulse.

The half-period with low-bias level, which precedes the application of high-bias, is much longer than the delay of release of carriers even from very deep trapping levels. The high-bias is thus applied when the trapping levels are completely depopulated; no afterpulsing can occur and thermally generated carriers generates the avalanche pulses. In fact, the statistical distribution of the measured delays has the characteristic exponential behavior of independent Poissonian events, clearly observable over three decades in Fig. 5. The primary dark-counting rate due to thermal generation of carriers is given by the reciprocal of the characteristic time constant of the exponential. Since fluctuations of the SPAD quality over the wafer can occur, a set of measurements has been performed for each process. For each geometry and size of SPAD device, at least 10 samples have been tested and the mean values obtained have been analyzed and compared, as shown in Fig. 6.

The improvement observed in the second generation is due to the substitution of the in situ n-doped polysilicon layer to the implanted one. The major improvement obtained in the third generation is due to the local gettering process. With a uniform defect concentration over the volume, a linear trend of dark count vs. active area is expected. Such a behavior

is indeed observed in the first and second generation, whereas in the third generation the decrease of dark-counting with decreasing area is super-linear. The effect is attributed to the fact that the local gettering ring is more efficient on the small devices, because it is closer to most of the detector active area [17].

A preliminary confirmation that the technology developed is suitable for the fabrication of integrated detector systems has been obtained. In tests carried out on small arrays, with 5×5 SPAD pixels of 20 μm diameter and 140 μm pitch, the experimental results, reported in Fig. 7, have shown very good uniformity of the SPAD features, at level suitable for obtaining larger arrays.

5. DETECTOR INTERNAL NOISE: AFTERPULSING

During an avalanche discharge deep levels in the depletion region can trap charge carriers. A carrier emitted by a trap at a later time, when the SPAD voltage is higher than the BV, can re-trigger the avalanche, thus producing a correlated after-pulse. The corresponding probability is called afterpulsing probability P_{ap} .

If the hold-off time enforced after each avalanche is long enough to cover the release of all trapped carriers, $P_{ap} = 0$ and afterpulsing is eliminated (see Sec.6). Such a long hold-off, however, implies a long counting dead-time, not suitable in many applications. If a shorter hold-off time is employed, the afterpulsing probability P_{ap} is finite and the total dark-counting-rate $C_{m,dark}$ is higher than the primary dark-counting-rate C_{th} :

$$C_{m,dark} = C_{th} + C_{th} \cdot P_{ap} + C_{th} \cdot (P_{ap})^2 + \dots + C_{th} \cdot (P_{ap})^n + \dots = C_{th} \cdot \sum_{n=0}^{\infty} (P_{ap})^n = C_{th} \cdot \frac{1}{1 - P_{ap}} \quad (1)$$

Minimizing the afterpulsing probability P_{ap} is a necessary requirement for a technology for SPAD fabrication and it is important being able to characterize P_{ap} rapidly and accurately. P_{ap} can be evaluated by two measurements of the dark-counting rate, first in actual operating conditions ($C_{m,dark}$) and then with a very long hold-off time (C_{th} , see Sec.6). However, the approach is fairly cumbersome and results are not very accurate. A different procedure, suitable for tests in industrial production of SPADs, was devised for obtaining an accurate characterization in a short time. The beam of a pulsed laser source was directed onto the SPAD, with power high enough to trigger an avalanche for each optical pulse. The repetition rate C_L of the laser pulses was much higher than the SPAD dark-counting-rate: $C_L \gg C_{m,dark} > C_{th}$. In these conditions the measured laser-induced avalanche rate $C_{m,laser}$ is:

$$C_{m,laser} = (C_{th} + C_L) \cdot \frac{1}{1 - P_{ap}} \quad (2)$$

and by combining (1) and (2) we obtain P_{ap} as

$$P_{ap} = 1 - \frac{C_L}{C_{m,laser} - C_{m,dark}} \quad (3)$$

The fast pulsed laser in Fig. 8 produces pulses at $\lambda=820\text{nm}$ with repetition rate $C_L=100\text{kHz}$, peak power 200mW, FWHM duration < 20 ps, corresponding to $\sim 10^6$ photons per pulse.

The AQC coupled to the SPAD was operating with 100ns hold-off time. Fig. 9 shows the afterpulsing probability measured as a function of the overvoltage for SPADs of different active areas. A linear relation between the overvoltage and the afterpulsing probability is observed. In fact, during the avalanche pulse only a very small fraction of the trap levels is filled, hence the probability for a carrier of being trapped is practically constant and the number of filled trap levels, n_{filled} , is proportional to the total number of charges Q_{av} in the avalanche pulse. The latter is proportional to the current, which is proportional to the overvoltage V_{over} [10]:

$$n_{filled} \propto Q_{av} \propto V_{over} \quad (4)$$

Eq. 4 points out that reducing the number of carriers flowing in the avalanche lowers the afterpulsing probability. AQC's instead of passive quenching circuits can be remarkably advantageous also from this standpoint [10].

Monolithic integration of SPAD and AQC, which is possible with the present technology, can make faster the avalanche quenching, thus reducing Q_{av} and the afterpulsing noise.

The afterpulsing probability level obtained in the present technology is adequate for many applications of SPADs. Furthermore, it has been checked that for obtaining P_{ap} well below 1% it is sufficient to operate with an hold off of 360ns, that is, with a counting dead-time suitable for any applications. Depending on the actual requirements in the desired application, a trade off can be established between dead-time and afterpulsing probability.

6. PHOTON TIMING

The SPAD performance in photon timing is characterized by its time resolution curve, which is the statistical distribution of the delay between the true arrival time of the photon and the measured time, marked by the onset of the avalanche current pulse. This curve, called briefly SPAD response, is obtained by means of a time-correlated single photon counting (TCSPC) apparatus [18], as shown in Fig. 10. Optical pulses with 820nm wavelength, less than 20 ps full-width at half-maximum (FWHM) and 10kHz repetition rate have been used in the measurements. We accurately verified that the contribution of the laser pulse and of the electronic jitter to the SPAD response are negligible. Fig. 11 shows an experimental histogram, characterized by a short peak followed by a slow tail [19]. The peak is due to photons absorbed in the depletion region and its width depends on the statistical fluctuations of the avalanche buildup time [20][21]. The tail is due minority carriers photogenerated in the neutral p region beneath the depletion layer that reach the junction by diffusion.

For SPADs directly built in substrates [19] the tail has shape dependent on the wavelength of the incident radiation, because the absorption coefficient is wavelength dependent. For SPAD structures in epitaxial layer with a lower junction, however, the tail is shorter [15] and can be reduced to exponential shape almost independent of wavelength, with time constant [14]:

$$\tau_D = \frac{W_{qn}^2}{\pi^2 D_n} \quad (5)$$

where W_{qn} is the thickness of the quasi neutral p region and D_n the diffusion coefficient for electrons. The neutral region thickness of our SPADs can be thus be checked, by substituting in (5) the experimental value of the time constant (τ_D). A thickness W_{qn} of $\sim 2.5\mu\text{m}$ is evaluated, in good agreement with the designed device structure.

Table 1 illustrates the SPAD timing resolution as a function of the overvoltage, for SPADs of different active areas. As expected, the jitter increases with the area of the photodetector and decreases as the overvoltage is increased [20][21]. The time resolution achieved at room temperature is remarkable, typically better than 80ps is for smaller devices. It can be improved by cooling the detector at temperatures easily accessible with commercially available Peltier coolers. Fig. 12 shows that at -20°C a $20\mu\text{m}$ SPAD attains 95ps FWHM, with a 21% improvement. At lower temperature the carrier mean free path is longer, carriers acquire higher energy from the electric field and have higher probability to impact ionize, the process of avalanche buildup becomes faster and has reduced statistical fluctuations.

7. QUANTUM DETECTION EFFICIENCY

The measurement principle adopted for testing the quantum detection efficiency (QE) of the SPADs is a direct comparison with a calibrated photodiode that receives the same photon flux. In order to keep the afterpulsing probability lower than 1%, thus making correction of the effect unnecessary, the dead-time of the AQC was set to 360 ns. The incident flux on the SPAD was limited, in order to keep the counting rate below $5 \cdot 10^4 \text{ s}^{-1}$. The corresponding mean time interval between two photons is 20 μs and, since an uncorrelated photon source is employed, there is less than 2% probability for a photon to arrive during a dead-time following a previous pulse. Correction of counting losses is therefore not necessary.

The instrumental apparatus, shown in Fig. 13, is a modified version of a system previously developed and employed for measuring the QE of CCD detectors. [22]

As illustrated in Fig. 14, the quantum detection efficiency was measured as a function of wavelength, with steps of 50 nm and with different overvoltage applied to the SPAD. It is worth noting that the in the near infrared good QE (>10%). This value might be improved because no anti reflection coating is used at the moment. Anyway, the obtained values are already very promising.

The linearity of the SPAD detector was also checked. These measurements were carried out up to significantly higher photon flux. Therefore, counting losses were corrected with the well-known equation for the effect of a constant, non-renewable dead-time [18]:

$$C_{est} = \frac{C_{meas}}{1 - T_{dead} C_{meas}} \quad (6)$$

where C_{meas} is the raw measured counting rate and C_{est} is the estimated counting rate, corrected from the losses due a dead time T_{dead} . As shown in Table 2, the SPAD response remains linear at least within two decimal digits as the photon flux is varied over an order of magnitude.

CONCLUSIONS

A new planar SPAD fabrication process, compatible with industrial CMOS technology, has been designed and tested. The development aims to the fabrication of large two-dimensional arrays of SPADs, to the monolithic integration on the same chip of SPAD detectors, active quenching circuits AQC, logic and/or memory circuits. The accurate characterization of the fabricated SPAD devices has confirmed that satisfactory performance is obtained. SPADs devices with 50µm diameter, operated at room temperature and at 10V excess bias, have dark-counting rate of 5kc/s, afterpulsing probability below 1% (with 360ns dead-time), quantum efficiency up to 50%, and 250ps photon timing resolution.

ACKNOWLEDGMENT

This work has been funded by CNR-IMM , Sezione di Catania through the European Project “EQUIS” IST- 1999-11594 and by STMicroelectronics. We wish to thank Markus Italia for the SRP measurement, Corrado Bongiorno for TEM analysis, Alessandro Piazza for the electrical measurements.

REFERENCES

- [1] T. A. Loui, G. Ripamonti and A. Lacaita, “Photoluminescence lifetime microscope spectrometer based in time correlated single photon counting with an avalanche diode detector”, *Rev. Sci. Instrum.*, vol.63, pp. 2994-2998, 1992.
- [2] S. Cova, A. Longoni, A. Andreoni, R. Cubeddu, “A semiconductor detector for measuring ultra-weak fluorescence decays with 70ps FWHM resolution”, *IEEE J. Quantum Electron.*, vol. QE-19, pp. 630-634, 1983.
- [3] A. Lacaita, P. A. Francese, S. Cova and G. Ripamonti, “Single-photon optical-time-domain reflectometer at 1.3 µm with 5 cm resolution and high sensitivity”, *Op. Lett.*, vol. 18, pp. 1110-1112, 1993.
- [4] F. Stellari, F.Zappa, S. Cova and L. Vendrame, “Tools for noninvasive optical characterization of CMOS circuits”, in *Proc. IEDM '99*, Washington, DC, Dec. 5-8,1999.
- [5] I. Procházka, K. Hamal and B. Sopko, “Photodiode based detector package for centimeter satellite laser ranging”, in *Proc. 7th Int. Workshop Laser Ranging Instrumentation*. Veillet, OCA-CERGA Grasse, 1990, ed., Matera, Italy, Oct. 2-8, 1989, pp.219-221.
- [6] M.Ghioni, S. Cova, I. Rech, F. Zappa, “Monolithic Dual-Detector for Photon-Correlation Spectroscopy With Wide Dynamic Range and 70-ps Resolution”, *IEEE J. of Quant. Elec.*, 37, 1588-1593, 2001.
- [7] Vasile, S.; Gothoskar, P.; Farrell, R.; Sdrulla, D. :”Photon detection with high gain avalanche photodiode arrays “, *IEEE Transactions on Nuclear Science*, 45, 720–723 (1998).

- [8] H. Kume, K. Koyama, N. Nakatsugawa, S. Suzuki and D. Fatlowitz, "Ultrafast microchannel plate photomultipliers", *Appl. Opt.*, vol. 27, pp. 1170-1178, 1988.
- [9] H. Dautet, P. Deschamps, B. Dion, A. D. MacGregor, D. MacSween, R. J. McIntyre, C. Trottier, and P. P. Webb, "Photon counting techniques with silicon avalanche photodiodes" *Appl. Opt.* n.32, pp 3894-3900, (1993)
- [10] S. Cova, M. Ghioni, A. Lacaita, C. Samori and F. Zappa "Avalanche Photodiodes and Quenching Circuits for Single Photon Detection" *Applied Optics*, vol.35, 1956-1976, 1996.
- [11] G. A. M. Hurx, H. C. de Graaff, W. J. Kloosterman and M. P. G. Knuvers, "A New Analytical Diode Model Including Tunneling and Avalanche Breakdown", *IEEE Trans. On Electron Devices*, vol. 39, no. 9, September 1992.
- [12] W.G. Oldham, R.R. Samuelson and P. Antognetti, "Triggering phenomena in avalanche diodes", *IEEE Trans. on Electron Devices*, vol. 19, no. 9, pp. 1056-1060 (1972).
- [13] S.Cova, A.Lacaita and G.Ripamonti: "Trapping phenomena in avalanche photodiodes on nanosecond scale", *IEEE Electron.Dev.Lett.* 12, 685-687, (1991)
- [14] A. Lacaita, M. Ghioni, S. Cova, "Double epitaxy improves single-photon avalanche diode performance", *Electronics Letters*, vol. 25, no. 13, 22 June 1989.
- [15] G.Ripamonti and S.Cova, "Carrier diffusion effects in the time-response of a fast photodiode", *Sol. State Electronics* 28, 925-931 (1985).
- [16] H.Hieslmair et al.: Chapter 15 for Emis Datareview EM 020 "Gettering of transition metals in silicon".
- [17] A.Zanchi, F.Zappa, M.Ghioni, "A probe detector for defectivity assessment in p-n junctions", *IEEE Trans. El. Dev.*, 47, pp. 609 -616 (2000).
- [18] V. O'Connor and D. Phillips, "Time-correlated Single Photon Counting", Academic Press, London, 1984.
- [19] S. Cova, G. Ripamonti and A. Lacaita, "Avalanche Semiconductor Detector for Single Optical Photons with a Time Resolution of 60 ps", *Nucl. Instr and Meth.*, vol A253, pp. 482-487, 1987.
- [20] A. Spinelli and A. L. Lacaita, "Physics and Numerical Simulation of Single Photon Avalanche Diodes", *IEEE Trans. On Electron Devices*, vol. 44, no. 11, November 1997.
- [21] A. Lacaita, M. Mastrapasqua, "Strong Dependence of Time Resolution on Detector Diameter in Single Photon Avalanche Diodes", *Electronic Letters*, vol. 26, no. 24, 22 November 1990.
- [22] Bonanno G., Bruno P., Cosentino R., Scuderi S., Bortoletto F., D'Alessandro M., Bonoli C., Fantinel D., Carbone A., Evola G, P. Amico and J. W Belectic, "TNG new generation CCD controller", *Optical detectors for Astronomy II*, Kluwer Academic Press, p. 387-393, 2000

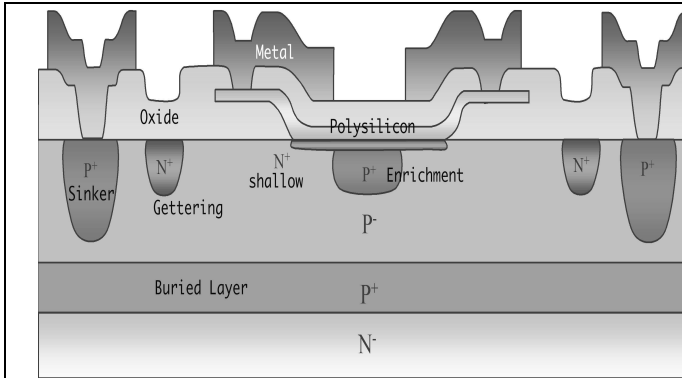


Fig. 1 Schematic cross section of a SPAD technology. The central part is the sensitive area of the detector, defined by the metal window and the central p+ doping.

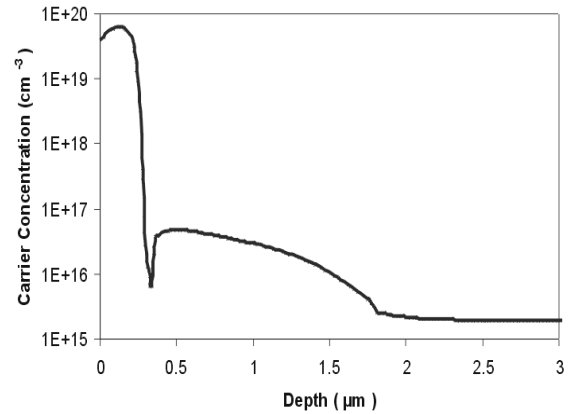


Fig. 2 Spreading resistance profile of the active area region.

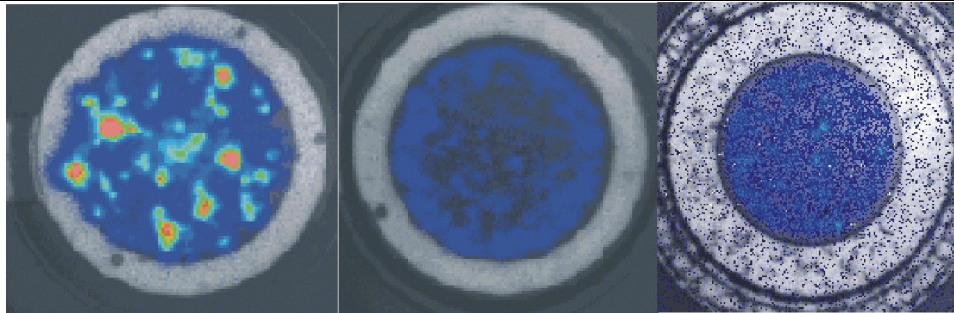


Fig. 3 Emission microscopy images of the three generations of SPADs. From the first, on the left, to the third, on the right, it is possible to recognize improvements regarding the uniformity of breakdown. No hot spots are present in the last generation.

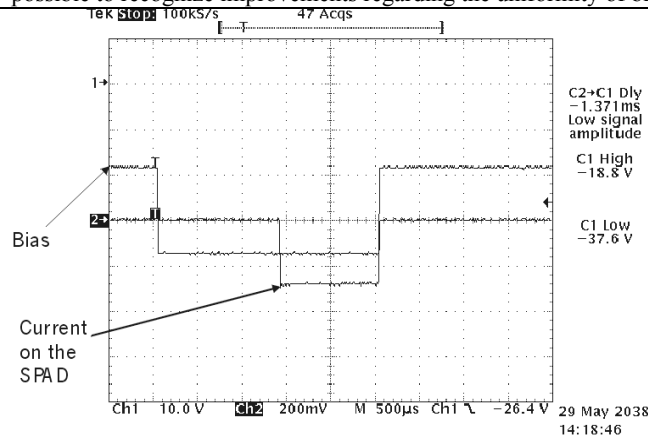


Fig. 4 Measurement on a digital oscilloscope of the time elapsed from the application of bias voltage above BV to the onset of the avalanche current pulse. The SPAD under test has 50 μm diameter and BV = 32.6 V.

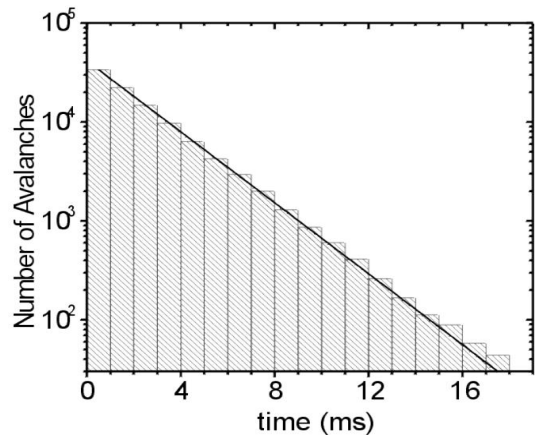


Fig. 5 Statistical distribution of measured delays for a SPAD device of the third generation, with the characteristic exponential behavior.

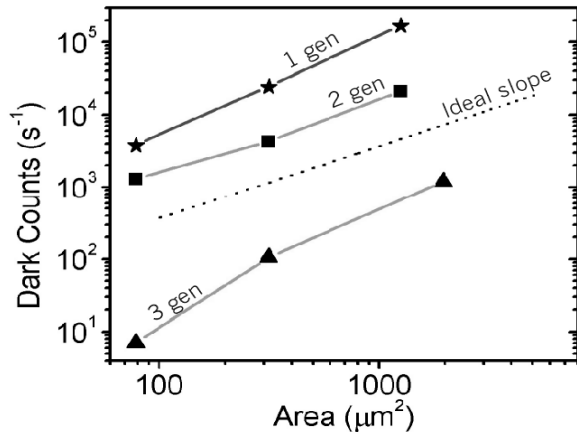


Fig. 6 Dark-counting rate vs. SPAD Active Area. Each data point is the mean value of measurements on 10 devices in different locations on a wafer, operated at 5V excess bias. Remarkably good uniformity was observed for the 3d generation devices.

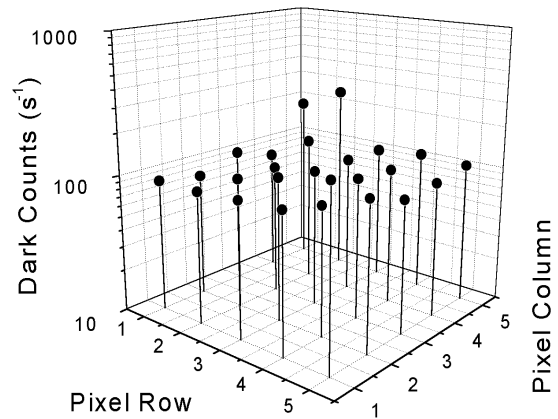


Fig. 7 Dark-counting rate for a 5x5 array of pixels of 20 μm diameter. The array has a square geometry and the distance between each column or row is 140 μm . Remarkable uniformity has been obtained.

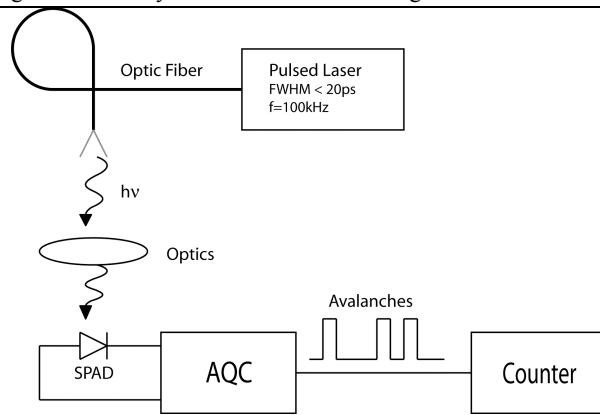


Fig. 8 Schematic picture of the measurement setup for afterpulsing.

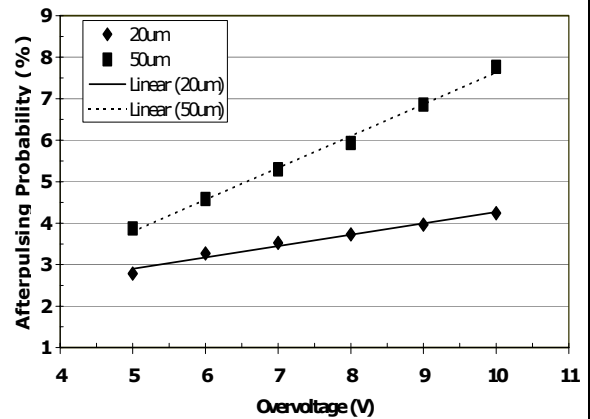


Fig. 9 Afterpulsing probability as a function of the overvoltage for SPAD devices with 20 μm and 50 μm diameter.

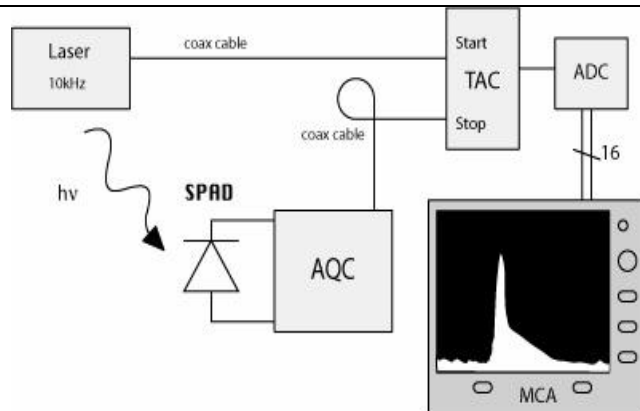


Fig. 10 Experimental set-up for the SPAD time-resolution test.

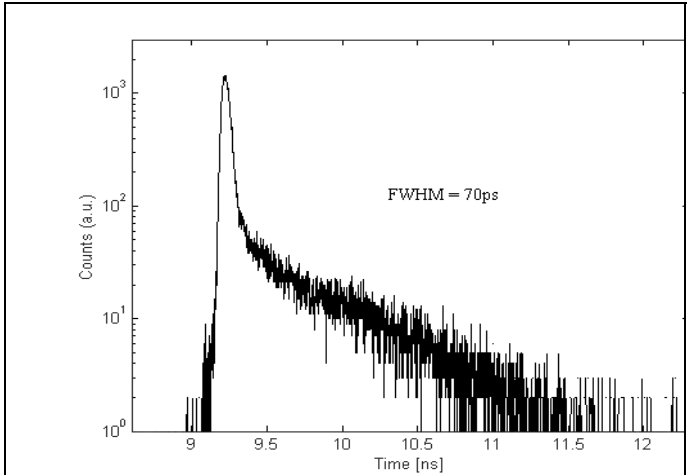


Fig. 11 Experimental time response of a SPAD with 10 μm diameter.

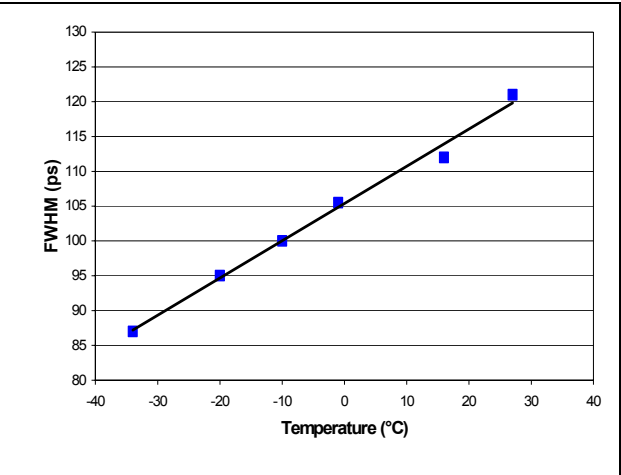


Fig. 12 FWHM of the SPAD response as a function of the temperature for a 20 μm diameter SPAD at 10V overvoltage.

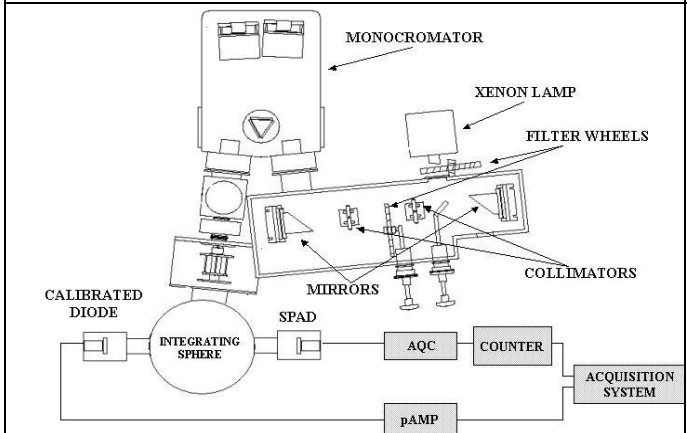


Fig. 13 Experimental set-up for measuring the quantum detection efficiency.

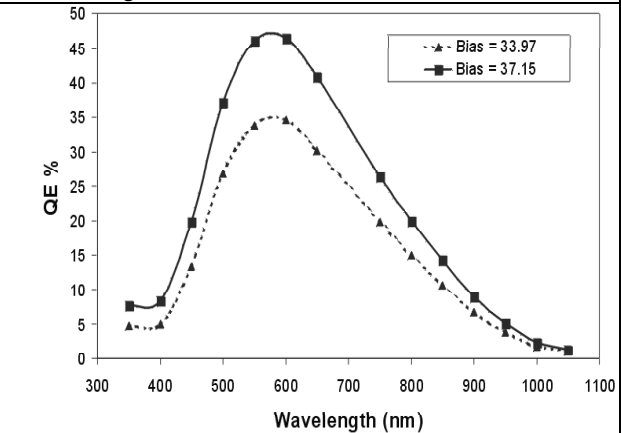


Fig. 14 Measured quantum detection efficiency vs. wavelength of a SPAD with 50 μm diameter, operated at 5V and 8V overvoltage.

Table 1 Typical timing resolution for SPADs with different active areas measured at three different overvoltages

SPAD Active Area	FWHM @5V	FWHM @10V	FWHM @ 13V
10 μm	161 ps	77 ps	74 ps
20 μm	184 ps	144 ps	113 ps
30 μm	236 ps	181 ps	165 ps
40 μm	285 ps	232 ps	188 ps
50 μm	330 ps	250 ps	-

Table 2 Linearity test of a SPAD in photon-counting

Photodiode (pA)	SPAD (count/s)	QE %	Deviation from linearity
1070	84866	46.08	1.002
906	71967	46.15	1.003
464.7	36678	45.86	0.997
122	9633	45.88	0.997